Optical Materials 33 (2010) 191–195

Contents lists available at ScienceDirect

Optical Materials

journal homepage: www.elsevier.com/locate/optmat

Spectroscopic analysis of Pr^{3+}:$Gd_3Ga_5O_{12}$ crystal as visible laser material

G.X. Cai, M. Zhou, Z. Liu, Z.Q. Luo, Y.K. Bu, H.Y. Xu, Z.P. Cai *, C.C. Ye

Department of Electronic Engineering, Xiamen University, 361005 Xiamen, PR China

ARTICLE INFO

Article history:
Received 30 May 2010
Received in revised form 6 September 2010
Accepted 30 September 2010
Available online 27 October 2010

Keywords:
Spectroscopy
Praseodymium
Garnet
Modified Judd–Ofelt theory

ABSTRACT

Pr^{3+}-doped $Gd_3Ga_5O_{12}$ single crystal is potentially good for generations of new lasers at visible range. The absorption and emission spectra of this crystal were measured at room temperature, as well as its fluorescence decay curves. Standard and modified Judd–Ofelt theories were used to analyze its intensity parameters, and the fluorescence properties for the $^3P_0$ emitting multiplet were predicted. To characterize the existence of the $^3P_0 \rightarrow {}^3F_3$ and $^3P_0 \rightarrow {}^3H_5$ transitions, which violate the selection rules of electric dipole transition, we also introduced the experimental branching ratio to reflect practical portion of transitions from $^3P_0$ multiplet. The stimulated emission cross sections of the promising laser transitions were then calculated and compared with other crystals which had realized efficient visible laser emissions. By analysing the spectroscopic properties we have showed that the Pr:GGG is an excellent candidate for solid state laser materials.

1. Introduction

The interest in Pr^{3+}-doped crystals stems from their special energy levels which might offer a great potential for lasing from blue to infrared regions. Recently, efficient visible laser emission has been obtained with fluoride crystals such as $LiYF_4$ (YLF) and $LiLuF_4$ (LLF) as well as $LiGdF_4$ (GLF) [1,2], and only with two oxide crystals $YAlO_3$ [3] and $Y_3Al_5O_{12}$ (YAG) [4] at room temperature and low temperature respectively. The laser action has been obtained in these host medium mainly because of their low phonon energy. Up to date, most oxide crystals are characterized by a relatively high energy cut-off of the phonon spectrum which often leads to a strong non-radiative decay of the $^3P_0$ level, quenching the upper laser level [2].

$Gd_3Ga_5O_{12}$ (GGG) is generally thought as an ideal laser host because of its excellent properties. First of all, it has a relatively high segregation coefficient. For example, the Lu^{3+} ions in a LLF, with the ionic radius of 1.12 Å, are very small compared to the doping Pr^{3+} ions which have an ionic radius of 1.27 Å, resulting in an enhanced possibility for crystal distortions and a low segregation coefficient. On the other hand, for a GLF, the Gd^{3+} ions are larger than the Lu^{3+} ions in a LLF (ionic radius of 1.19 Å cf. 1.12 Å), allows relatively high Pr^{3+} (1.27 Å) doping levels in the crystal with reduced amounts of defects. The segregation coefficients of Pr^{3+} in the LLF and the GLF crystals are ~0.15 and 0.39, respectively [2]. For a GGG which is a garnet oxide, fortunately, it is similar to a GLF in terms of the smaller difference in the ionic radii Gd^{3+} (1.07 Å) and the doping Pr^{3+} (1.14 Å). It makes Pr:GGG a high segregation coefficient, which is 0.64. Meanwhile, GGG is transparent from UV to mid-IR bands and has a high index of refraction. These properties are favorable to radiative transitions in Pr^{3+} ion. More importantly, the low phonon energy associated with GGG host (the maximum phonon energy of the optical phonon is ~600 cm^{-1}) [5] would help to generate visible laser oscillations at room temperature.

In this present contribution, the absorption and fluorescence spectra and fluorescence decay curves of the Pr^{3+}-doped GGG single crystal (Pr:GGG) have been recorded at room temperature (RT). The standard and modified Judd–Ofelt (J–O) theories have been performed to analyze the absorption spectrum to determine the Judd–Ofelt (J–O) intensity parameters Ω_t ($t = 2$, 4 and 6), and the spontaneous transition probabilities, fluorescence branching ratios and radiative lifetimes were obtained. The stimulated emission cross sections of the promising laser transitions have also been studied.

2. Experiments

The Pr:GGG was grown by the Czochralski technique, in which the nominal concentration of praseodymium ions was 1 at.%. Considering the segregation coefficient of Pr^{3+} in the GGG crystal, the actual Pr^{3+} concentration is 0.81×10^{20} cm^{-3}. The Pr:GGG crystal sample used for spectroscopic measurements was optically polished to flat and parallel faces, with dimensions of $3 \times 3 \times 2$ mm^3. The room temperature absorption spectrum was measured using a Perkin–Elmer UV–vis–NIR spectrometer (Lambda-750). The emission spectrum was recorded from 480 nm to 760 nm when the crystal was excited by a NICHIA blue laser diode operating at

* Corresponding author. Tel.: +86 592 2580071; fax: +86 592 2580040.
E-mail address: zpcai@xmu.edu.cn (Z.P. Cai).

0925-3467/$ - see front matter © 2010 Elsevier B.V. All rights reserved.
doi:10.1016/j.optmat.2010.09.031

450 nm. Pr^{3+} irons were pumped into their $^3P_2$ states. A photomultiplier tube (PMT) located at the output slit of a 50 cm focal length monochromator was used to detect the fluorescence emission intensity at room temperature. The spectral resolution is 0.1 nm. For lifetime measurements, an Edinburgh Instruments F900 was used to measure the decay curves of the $^3P_0$ multiplet based on the measurement principle of time correlated single photon counting (TCSPC), which provides high quality for fluorescence lifetime analyses.

The refractive indices of GGG crystal come from Ref. [6] where a Sellmeier equation was fitted. The values of the refractive indices versus wavelength were employed in the following spectroscopic analysis to make results more accurate.

3. Results and discussion

3.1. Absorption spectrum and Judd–Ofelt analysis

The room temperature absorption spectrum for Pr:GGG crystal is shown in Fig. 1. The base line in the spectrum, which is caused by the reflection of the crystal surface and the defects in the crystal, has been corrected. The absorption bands correspond to the transitions from the ground multiplet $^3H_4$ to higher excited multiplets, which were assigned and shown in Fig. 1. It can be seen that the maximum absorption peak is centered at 450 nm and a series of strong absorption bands are located between 435 and 500 nm. Therefore the Pr:GGG crystal can be effectively pumped by a blue diode laser or a blue solid state laser, and all the 4f–4f transitions can be excited.

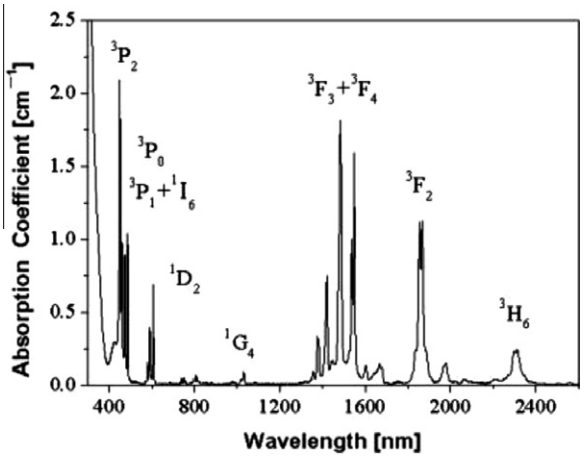

Fig. 1. Absorption spectrum of Pr:GGG crystal at RT. The transitions are assigned to be from the $^3H_4$ ground multiplet to the indicated multiplets.

The J–O theory [7,8] was then adopted to analyze the measured room temperature absorption spectrum. As shown in Fig. 1, we assigned eight absorption bands from $^3H_4$. The overlapping absorption bands, such as $^3P_1 + {}^1I_6$ and $^3F_3 + {}^3F_4$, were treated as one band. The experimental line strengths S_{exp} were evaluated. While only the electronic dipole transitions were considered, they were fitted to the theoretically calculated line strengths S_{cal} following a standard J–O procedure and the J–O intensity parameters were obtained. These values of line strengths were listed in Table 1 and J–O parameters in Table 2. The doubly reduced matrix elements of the unit tensor operator adopted here come from Ref. [9] since they are almost independent of the host crystal. For the overlapping absorption transitions, the sum of the corresponding matrix elements is used.

The negative or small values for Ω_2 in Pr^{3+}-doped crystal have been reported in many literatures [10,11]. The problem was also encountered in our work when attempted to fit all the absorption transition bands with the same set of J–O parameters. While omitting the $^3H_4 \rightarrow {}^3P_2$ absorption transition, the value of Ω_2 is still small but with a reasonable deviation between experimental and calculated line strengths. The reason that standard J–O theory works less well in Pr^{3+}-doped crystal lies in the breakdown of approximation made by this theory, which contains two aspects: all the states of the disturbing 4f5d configuration are degenerate and their energy positions are much higher than those of 4f–4f transitions. The neglect of the $^3H_4 \rightarrow {}^3P_2$ absorption transition may attenuate the second problem without solving the first one [10].

Several modifications to the standard J–O theory have been developed by researchers to find more reliable and reasonable intensity parameters for Pr^{3+}. A procedure introduced by Quimby and Miniscalco [11], which incorporates the measured fluorescence branching ratios into the fitting, is shown to improve agreement with experiment. A theory devised by Kornienko et al. [12], which takes into account the energy dependence of the multiplets involved in the transition with the energy of the 4f5d configuration, retrieves the approximation of J–O theory in Pr^{3+} analysis.

Table 2
J–O parameters of Pr:GGG under different procedure.

		Standard theory		Modified theory	
		$^3P_2$ included	$^3P_2$ omitted	$^3P_2$ included	$^3P_2$ omitted
Intensity parameters ($\times10^{-20}$ cm^2)	Ω_2	0.13	0.26	0.92	1.24
	Ω_4	2.33	2.46	2.14	2.27
	Ω_6	2.53	2.12	3.82	3.12
RMS ΔS ($\times10^{-20}$)	ΔS_{rms}	1.66	0.22	1.57	0.20

Table 1
Measured and calculated absorption line strengths of Pr:GGG.

Transition (from $^3H_4$)	λ_{mean} (nm)	S_{exp} ($\times10^{-20}$ cm^2)	S_{cal} ($\times10^{-20}$ cm^2)			
			Standard theory		Modified theory	
			$^3P_2$ included	$^3P_2$ omitted	$^3P_2$ included	$^3P_2$ omitted
$^3H_6$	2309.1	0.37	0.43	0.38	0.42	0.36
$^3F_2$	1875.1	1.37	1.30	1.37	1.27	1.37
$^3F_3 + {}^3F_4$	1499.5	3.49	3.93	3.51	4.07	3.51
$^1G_4$	1026.3	0.07	0.08	0.07	0.10	0.08
$^1D_2$	597.3	0.60	0.17	0.15	0.23	0.19
$^3P_0$	487.6	0.44	0.40	0.42	0.38	0.40
$^3P_1 + {}^1I_6$	474.3	0.58	0.58	0.60	0.60	0.62
$^3P_2$	441	4.08	0.43	–	0.63	–

Quimby's method requires additional experimental fluorescence measurements and more complicated fitting procedure than standard theory. Since the number of the available measured absorption bands is seven or eight, which is sufficient to obtain reliable J–O intensity parameters, we adopt the Kornienko's modified theory to execute further analysis. The theoretically calculated line strength of an electric dipole transition is expressed by introducing a weight-factor in this modified theory,

$$S_{\mathrm{cal}}^{\mathrm{modified}}(J \to J') = \sum_{t=2,4,6} \Omega_t |\langle (S,L)J \| U^{(t)} \| (S',L')J' \rangle|^2 \times [1 + 2\alpha(E_J + E_{J'} - 2E_f^0)] \quad (1)$$

Where E_J and $E_{J'}$ are the energy of the initial and final multiplets, respectively, E_f^0 is the center energy of all the 4f–4f states, which equals 9940 cm^{-1} for Pr^{3+} ions, and the Ω_t and α parameters can be obtained from the J–O least square fitting. Since it seems better not to let α parameter vary freely [13], a fixed value of 1.0×10^{-5} is used for α in this work, which is calculated by the following formula,

$$\alpha = \frac{1}{2\Delta_{5d}} = \frac{1}{2(E_{4f5d} - E_f^0)} \quad (2)$$

where E_{4f5d} is the energy of the lowest 4f5d state, and Δ_{5d} is the energy difference between the energy of the lowest 4f5d state and the center energy of all the 4f–4f states. For Pr^{3+} ion, Δ_{5d} is about 50,000 cm^{-1} [12]. It would be almost the same in Pr:GGG crystal since the energy difference will not be influenced by the crystal field.

The results of the modified J–O theory are also listed in Table 1 and 2. It can be seen clearly that the modified J–O analysis with the $^3H_4 \to {}^3P_2$ absorption transition omitted yielded the least root-mean-square deviation and more reasonable value of Ω_2. This group of J–O intensity parameters will be adopted to the following fluorescence analysis.

3.2. Fluorescence spectra and lifetimes

The room-temperature emission spectrum of Pr:GGG excited by 450 nm pumping is shown in Fig. 2. The fluorescence in the visible region mainly consists of emissions from the $^3P_0$ multiplet, as shown in Fig. 2. It can be predicted that the infrared emissions originating from $^3P_0$ multiplet would be very weak. Those transitions will be ignored in our analysis. Although there are the transitions originating from $^3P_1$ and $^1D_2$ multiplets, they are weak and some of them overlap with the emissions from the $^3P_0$ multiplets. Therefore they are neglected in the following analysis.

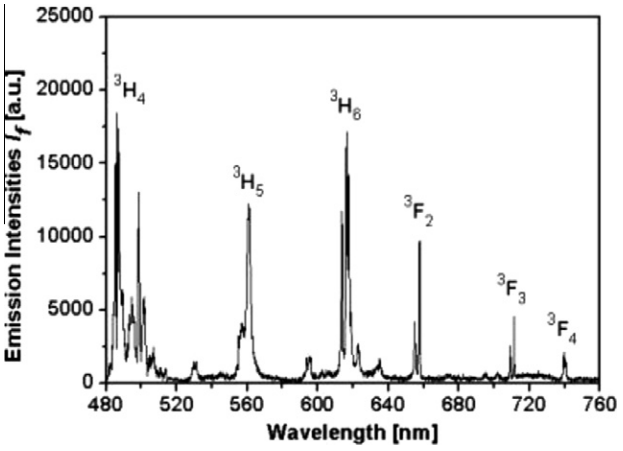

Fig. 2. Fluorescence spectrum of Pr:GGG at RT. The transitions are assigned to be from the $^3P_0$ multiplet to the indicated multiplets.

Based on the modified J–O theory, the spontaneous transition probability of an electric dipole transition will be given by the following expression,

$$A(J \to J') = \frac{64\pi^4 e^2}{3h(2J+1)\bar{\lambda}_{\mathrm{em}}^3} \frac{n(n^2+2)^2}{9} S_{\mathrm{cal}}^{\mathrm{modified}}(J \to J') \quad (3)$$

The fluorescence branching ratio β and radiative lifetime τ_{rad} will be predicted in the same way when the standard theory is used. The results of the $^3P_0$ transitions are listed in Table 3, and τ_{rad} is calculated to be 28.6 μs.

It is worth noting that from Table 3 the line strengths and consequently the transition probabilities of $^3P_0 \to {}^3F_3$ and $^3P_0 \to {}^3H_5$ transitions were calculated to be zero. These predicted results were in conflict with the measured emission spectrum presented in Fig. 2. In fact, $^3P_0 \to {}^3F_3$ and $^3P_0 \to {}^3H_5$ transitions violate the selection rules of electric dipole transition since their matrix elements equal to zero. The reason they can be measured in emission spectra is the mixing of multiplets causing by the even-parity crystal field [14]. In order to show clearly their existence, we calculated experimentally the branching ratio $\beta_{JJ'\text{-exp}}$ by integrating the relative fluorescence spectra as following [15],

$$\beta_{JJ'-\mathrm{exp}} = \frac{\int_{J\to J'} \lambda I(\lambda) d\lambda}{\sum_{J'} \int_{J\to J'} \lambda I(\lambda) d\lambda} \quad (4)$$

Where I is the fluorescence intensity, and λ the wavelength. The value of $\beta_{JJ'\text{-exp}}$ for transitions from $^3P_0$ multiplet are also listed in Table 3. It can be found that the relationship between these transitions varied and the branching ratio of $^3P_0 \to {}^3F_2$ transition sharply reduced to be less than that of $^3P_0 \to {}^3H_6$. This set of data reflects the real stimulated emission situation of the Pr:GGG crystal.

Room temperature decay curve of the transition $^3P_0 \to {}^3H_6$ is shown in Fig. 3 in semilog scale. The measured emission wavelength was 616.3 nm while the excitation wavelength was 450 nm. The linear relationship in the figure demonstrates a single exponential decay behavior of the fluorescence. The measured fluorescence lifetime, τ_f, of the $^3P_0$ multiplet is 23.1 μs, obtained by fitting the decay curve.

Then the fluorescence quantum efficiency $\eta = \tau_f/\tau_{\mathrm{rad}}$ of the $^3P_0$ multiplet is calculated to be 80.8%, which is comparable to 91% for $Pr:Sr_5(PO_4)_3F$ [16] and higher than that for other Pr^{3+}-doped oxide crystals [17–19]. The high quantum efficiency of Pr:GGG crystal is attributed to the small phonon energy of the GGG crystal (~600 cm^{-1}, as mentioned above) and the low Pr^{3+} concentration in the sample, which make the multi-phonon relaxation and the concentration quenching, respectively, weak.

Fluorescence lifetimes of other transitions from the $^3P_0$ multiplet were also measured and analyzed in the same way. All of them also display single exponential behaviors. The measured results for

Table 3
Predicted radiative properties of Pr:GGG at RT including spontaneous transition probabilities, fluorescence branching ratios and radiative lifetime. The experimental branching ratios are also tabulated.

Transition (from $^3P_0$)	λ_{mean} (nm)	S_{cal} ($\times 10^{-20}$ cm^2)	$A_{JJ'}$ (s^{-1})	$\beta_{JJ'\text{-cal}}$ (%)	$\beta_{JJ'\text{-exp}}$ (%)
$^3F_4$	739.9	0.32	3351	9.4	2.6
$^3F_3$	711.2	0	0	0	3.8
$^3F_2$	656.1	0.41	6817	19.2	5.8
$^3H_6$	617.5	0.25	4876	13.7	25.0
$^3H_5$	558.8	0	0	0	22.7
$^3H_4$	493.2	0.40	19,960	56.2	40.1
				ΣA = 35,004 s^{-1}, τ_{rad} = 28.6 μs	

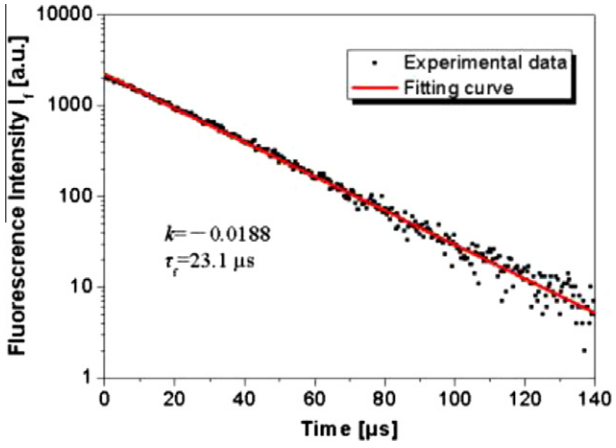

Fig. 3. RT fluorescence decay curve of Pr:GGG crystal plotted in semilog scale, excited at 450 nm and recorded at 616.3 nm. The points and line represent the experimental data and linearly fitting result, respectively.

the $^3P_0 \rightarrow {}^3H_5$, $^3P_0 \rightarrow {}^3H_6$ and $^3P_0 \rightarrow {}^3F_2$ transitions are listed in Table 4. One can find that these transitions have almost the same fluorescence lifetimes, since they are from the same $^3P_0$ multiplet.

3.3. Stimulated emission cross sections

The stimulated emission cross section σ_{em} is an important parameter which indicates the laser properties of a crystal. It can be calculated from the room temperature fluorescence spectra by the Füchtbauer–Ladeburg (F–L) formula [15]. To obtained more accurate and reliable results of σ_{em}, both measured $\beta_{JJ'\text{-exp}}$ and τ_{exp} are used in the F–L formula. Three groups of σ_{em} are calculated and shown in Fig. 4, corresponding to these three transitions: $^3P_0 \rightarrow {}^3H_5$, $^3P_0 \rightarrow {}^3H_6$ and $^3P_0 \rightarrow {}^3F_2$. The peak stimulated emission cross sections and the corresponding wavelengths are listed in Table 4. It can be found that the $^3P_0 \rightarrow {}^3H_6$ as red laser channel has the largest peak emission cross section, which is 15.3×10^{-20} cm^2 at 616.3 nm.

Table 4
Radiative lifetime and peak emission cross section of Pr:GGG. The quantum efficiencies are also calculated.

Transition	τ_{rad} (μs)	τ_{exp} (μs)	η (%)	λ_{peak} (nm)	$\sigma_{em\text{-}peak}$ ($\times 10^{-20}$ cm^2)
$^3P_0 \rightarrow {}^3H_5$	28.6	22.5	78.7	560.8	6.9
$^3P_0 \rightarrow {}^3H_6$	28.6	23.1	80.8	616.3	15.3
$^3P_0 \rightarrow {}^3F_2$	28.6	22.5	78.7	657.7	12.4

Table 5
Comparison of peak emission cross sections between Pr^{3+}-doped crystals.

Transition	$\sigma_{em\text{-}peak}$ ($\times 10^{-20}$ cm^2) [λ (nm)]			
	Pr:GGG (1%)	Pr:$YAlO_3$ (1%)	Pr:YLF (0.65%)	Pr:LLF (0.45%)
$^3P_0 \rightarrow {}^3H_6$	15.3 [616.3]	64 [613.9]	14 [≈607]	12 [≈607]
$^3P_0 \rightarrow {}^3F_2$	12.4 [657.7]	15 [662.4]	22 [≈640]	21 [≈640]
Ref.	Present work	[3]	[2]	[2]

Pr:GGG bears great potential to be an excellent laser crystal. This can be seen from Table 5, which compares the peak stimulated emission cross sections of four Pr^{3+}-doped crystals. Laser oscillations have been realized using crystals of Pr:$YAlO_3$, Pr:YLF and Pr:LLF. Since the peak σ_{em} of Pr:GGG has the same scale as these crystals, there are great probability of lasing in these two transitions for Pr:GGG.

4. Conclusions

In this contribution, we have investigated the optical properties of Pr:GGG single crystal. The absorption spectrum was analyzed using both the standard and modified J–O theories. The modified J–O theory with the $^3H_4 \rightarrow {}^3P_2$ transition omitted results in the least deviation. The J–O intensity parameters were calculated to be: $\Omega_2 = 1.24 \times 10^{-20}$ cm^2, $\Omega_4 = 2.27 \times 10^{-20}$ cm^2, $\Omega_6 = 3.12 \times 10^{-20}$ cm^2.

As the predicted branching ratios were inconsistent with the measured emission spectra, we calculated the branching ratios using the experimental data. The results reflect the real stimulated emission situation.

The fluorescence lifetimes of the typical transitions from the $^3P_0$ multiplet were experimentally determined. The results show single exponential behaviors of the fluorescence decay for the $^3P_0$ multiplet, which means that there is no energy transfer involved in the $^3P_0$ transition. The room temperature fluorescence lifetime and quantum efficiency of Pr:GGG are 23.1 μs and 80.8%, respectively.

Both experimental $\beta_{JJ'\text{-exp}}$ and τ_{exp} are used to calculate the stimulated emission cross sections. It can be found that the peak stimulated emission cross section of the $^3P_0 \rightarrow {}^3H_6$ as red laser channel is 15.3×10^{-20} cm^2, which is the largest emission cross section among all the emission bands of Pr:GGG crystal. By comparing with other Pr^{3+}-doped crystals which have realized their laser oscillations, it can draw a conclusion that the Pr:GGG is an excellent candidate for solid state laser materials.

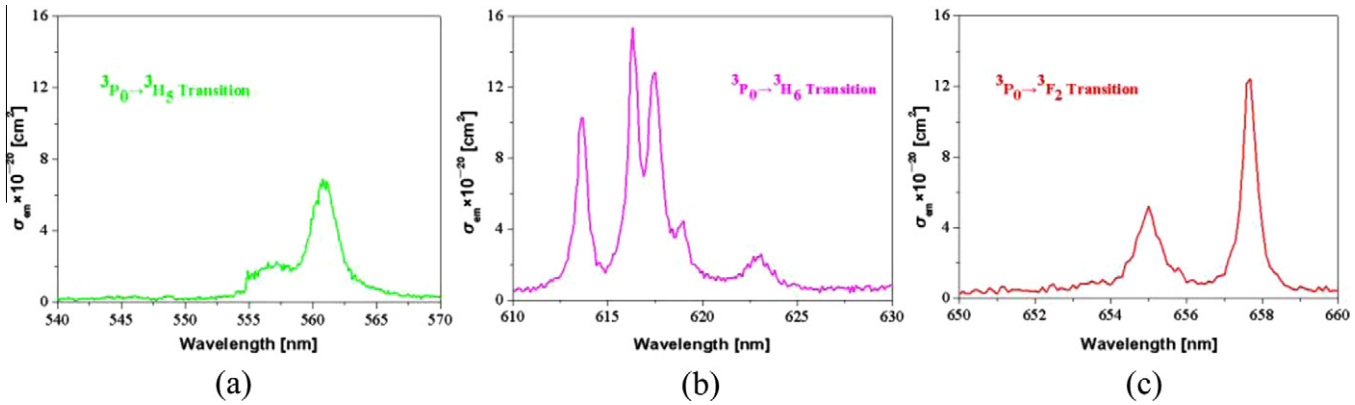

Fig. 4. Stimulated emission cross section of (a) the $^3P_0 \rightarrow {}^3H_5$ transition; (b) the $^3P_0 \rightarrow {}^3H_6$ transition; (c) the $^3P_0 \rightarrow {}^3F_2$ transition.

Acknowledgements

The authors would like to thank Professor Chaoyang Tu, Fujian Institute of Research on the Structure of Matter, Chinese Academy of Sciences, for providing the Pr:GGG crystal. And we also appreciate the help from Dr. Hui Xu, Zhejiang University, for measuring the fluorescence decay of this crystal.

References

[1] F. Cornacchia et al., Optics Express 15 (2007) 992.
[2] F. Cornacchia et al., Optics Express 16 (2008) 15932.
[3] T. Danger, A. Bleckmann, G. Huber, Applied Physics B: Lasers and Optics 58 (1994) 413.
[4] M. Malinowski, M.F. Joubert, B. Jacquier, Physica Status Solidi (A) 140 (1993) K49.
[5] R. Naccache et al., The Journal of Physical Chemistry. C 112 (2008) 7750.
[6] D.K. Sardar et al., Journal of Applied Physics 93 (2003) 2602.
[7] B.R. Judd, Physical Review 127 (1962) 750.
[8] G.S. Ofelt, The Journal of Chemical Physics 37 (1962) 511.
[9] A.A. Kaminskii, Laser Crystals, Their Physics and Properties, Springer, Berlin, 1981.
[10] B.E. Bowlby, B.D. Bartolo, Journal of Luminescence 100 (2002) 131.
[11] R.S. Quimby, W.J. Miniscalco, Journal of Applied Physics 75 (1994) 613.
[12] A.A. Kornienko, A.A. Kaminskii, E.B. Dunina, Physica Status Solidi (B) 157 (1990) 267.
[13] P. Goldner, F. Auzel, Journal of Applied Physics 79 (1996) 7972.
[14] G. Liu, B. Jacquier, Spectroscopic Properties of Rare Earths in Optical Materials, Springer, Berlin, 2005.
[15] B. Aull, H. Jenssen, IEEE Journal of Quantum Electronics 18 (1982) 925.
[16] D.K. Sardar, F. Castano, Journal of Applied Physics 91 (2002) 911.
[17] L.D. Merkle et al., Journal of Applied Physics 79 (1996) 1849.
[18] S. Pinelli et al., Optical Materials 25 (2004) 91.
[19] F.B. Xiong, Z.D. Luo, Y.D. Huang, Applied Physics B: Lasers and Optics 80 (2005) 321.